The Meteoritical Society

Meteoritics & Planetary Science 42, Nr 10, 1763–1779 (2007)
Abstract available online at http://meteoritics.org

Mineralogy, petrology, and shock history of lunar meteorite Sayh al Uhaymir 300: A crystalline impact-melt breccia

J. A. HUDGINS[1*], E. L. WALTON[2], and J. G. SPRAY[1]

[1]Planetary and Space Science Centre, Department of Geology, University of New Brunswick, 2 Bailey Drive, Fredericton, New Brunswick E3B 5A3, Canada
[2]Department of Earth and Atmospheric Sciences, 1-26 Earth Sciences Building, University of Alberta, Edmonton, Alberta T6G 2E3, Canada
[*]Corresponding author. E-mail: jillian.hudgins@unb.ca

(Received 12 January 2007; revision accepted 26 April 2007)

Abstract–Sayh al Uhaymir (SaU) 300 comprises a microcrystalline igneous matrix (grain size <10 μm), dominated by plagioclase, pyroxene, and olivine. Pyroxene geothermometry indicates that the matrix crystallized at ~1100 °C. The matrix encloses mineral and lithic clasts that record the effects of variable levels of shock. Mineral clasts include plagioclase, low- and high-Ca pyroxene, pigeonite, and olivine. Minor amounts of ilmenite, FeNi metal, chromite, and a silica phase are also present. A variety of lithic clast types are observed, including glassy impact melts, impact-melt breccias, and metamorphosed impact melts. One clast of granulitic breccia was also noted. A lunar origin for SaU 300 is supported by the composition of the plagioclase (average An_{95}), the high Cr content in olivine, the lack of hydrous phases, and the Fe/Mn ratio of mafic minerals. Both matrix and clasts have been locally overprinted by shock veins and melt pockets. SaU 300 has previously been described as an anorthositic regolith breccia with basaltic components and a granulitic matrix, but we here interpret it to be a polymict crystalline impact-melt breccia with an olivine-rich anorthositic norite bulk composition. The varying shock states of the mineral and lithic clasts suggest that they were shocked to between 5–28 GPa (shock stages S1–S2) by impact events in target rocks prior to their inclusion in the matrix. Formation of the igneous matrix requires a minimum shock pressure of 60 GPa (shock stage >S4). The association of maskelynite with melt pockets and shock veins indicates a subsequent, local 28–45 GPa (shock stage S2–S3) excursion, which was probably responsible for lofting the sample from the lunar surface. Subsequent fracturing is attributed to atmospheric entry and probable breakup of the parent meteor.

INTRODUCTION

Sayh al Uhaymir (SaU) 300, a stone weighing 152.46 g, was discovered on a gravel plateau of Miocene limestone, 42 km south-southeast of Ghaba, Oman, on February 21, 2004 (Bartoschewitz et al., unpublished data). It is flat and rounded, olive green in color, with a resinous luster and minor rust patches, and no relict fusion crust. In hand specimen, the cut surface reveals clasts set within a fractured matrix pervaded by rust-colored stains, dark melt veins (10–300 μm wide), metal specks, and vesicles (<2 mm) filled with white alteration products. SaU 300 was originally described in an abstract by Bartoschewitz et al. (unpublished data) as a lunar anorthositic highland regolith breccia with basaltic and meteoritic components. Noble gas isotope data reveal a paucity in solar wind components, which was interpreted by Bartoschewitz et al. (unpublished data) to indicate that most of the noble gases were lost by a heating event. The cosmic ray exposure age, based on the stable noble gas isotope ^{3}He, was calculated to be 0.2 Ma (Bartoschewitz et al., unpublished data), putting an upper limit on the transit time from the Moon to Earth. U/Th-He (age of supposed thermal metamorphism) and K-Ar (lower limit of crystallization age) results suggest events at 0.055 and 2.9 Ga, respectively (Bartoschewitz et al., unpublished data).

The Moon has been directly sampled at the six Apollo (USA) and the three Luna (Soviet) sites, all confined to a restricted region of the equatorial nearside, defining a polygon covering ~4.4% of the lunar surface (Warren and Kallemeyn 1991). Remote-sensing studies have shown that this area is enriched in incompatible heat-producing elements; therefore, material obtained from this region may not be

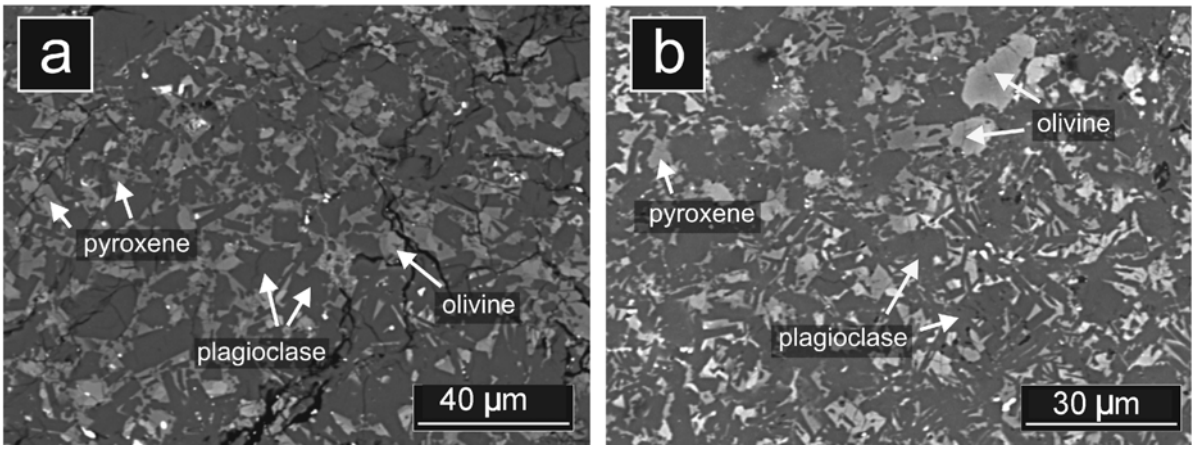

Fig. 1. BSE images of the matrix of SaU 300. a) Three main phases are plagioclase, pyroxene, and olivine. b) Olivine shows reaction texture (anhedral to subhedral shapes). White phases are FeNi metal.

representative of the average lunar crust (Jolliff et al. 2000; Korotev 2005). Additional samples of the Moon exist as meteorites, delivered by impact events that ejected material at a velocity in excess of 2.4 km/s from the lunar near surface. Lunar meteorites (lunaites) provide researchers with samples from random locations, most of which are probably far removed from those sampled by humans (e.g., Gnos et al. 2004). Meteorites are therefore probably more representative of the average lunar crust, as opposed to the spatially restricted samplings of the Apollo and Luna missions. Combined with the Apollo and Luna material, meteorites can be used as a ground truth for remotely sensed data (Korotev 2005). The increase in lunar meteorite recovery, about 44 since the year 2000, is mainly due to the intensive search for meteorites, particularly in the North African and Arabian deserts and in Antarctica. The exact number of lunar meteorites is unknown due to unestablished pairing relationships for the newest meteorites, but there are currently about 100 named lunar meteorites, of which about 50 have been paired (Korotev 2005).

The complex textures of lunar meteorites require careful petrographic characterization (e.g., Cohen et al. 2004). This is well demonstrated by Meteorite Hills (MET) 01210 and Pecora Escarpment (PCA) 02007. Initially classified as a lunar feldspathic regolith breccia and a basaltic lunar breccia, respectively, they were later reclassified as predominantly basaltic (MET 01210) and feldspathic (PCA 02007) regolith breccias (Day et al. 2006). At present, there is a need for comprehensive, peer-reviewed descriptions of lunar samples to keep the database current and accurate as new material is recovered, and to establish pairing relationships. Here we present an investigation of the mineralogy, petrology, and bulk composition of SaU 300, a meteorite originally classified as an anorthositic regolithic granulite breccia (Hsu et al. 2006; Bartoschewitz et al., unpublished data), with implications for its pairing relationships, formation (impact) history, and prelaunch location.

ANALYTICAL METHODS

This study is based on the examination of two thin sections of SaU 300 (section 30.1285.6, 1.5 × 0.8 cm; section 30.1285.5, 1.4 × 0.85 cm) supplied by the collector. We initially examined each doubly polished thin section with an optical microscope. Backscattered electron (BSE) images and quantitative mineral analyses were obtained at the University of New Brunswick (UNB) using energy dispersive spectroscopy (EDS) with a JEOL 6400 analytical scanning electron microscope (ASEM) equipped with an EDAX Phoenix X-ray microanalysis system possessing a Sapphire Si (Li) detector and Genesis microanalysis software. Operating conditions were 15 kV accelerating voltage and 1.5 nA current, at working distances of 7–14 mm. Count times were 50 s. ZAF corrections were applied to all analyses. Analyses were calibrated using a multi-element standard block (type 202-52). We obtained BSE and secondary electron (SE) images of SaU 300 melt veins and melt pockets using a JEOL 6301F field emission SEM (FE-SEM) at the University of Alberta (UA). The FE-SEM was operated at 20 kV, 10 nA, and a working distance of 8 mm. Melt glasses (pockets and veins) and certain mineral and lithic clasts were analyzed at UA using a JEOL 8900 electron microprobe (EMP) equipped with five wavelength dispersive spectrometers (WDS) using an accelerating voltage of 15 or 20 kV at a beam current of 15 or 20 nA. Minerals were analyzed using a 1 μm spot size. A defocused beam (3–10 μm in diameter) was deployed to minimize alkali metal mobilization in glasses and certain mineral phases (Spray and Rae 1995). Natural minerals and glasses were used as standards for all EMP analysis.

We estimated the bulk rock composition of SaU 300 by raster scanning 50 separate 170 × 120 μm areas using ASEM (see Walton et al. 2006 for analytical details). EDS, rather than WDS, was used because of its ability to minimize alkali metal migration (Spray and Rae 1995). Totals were low due

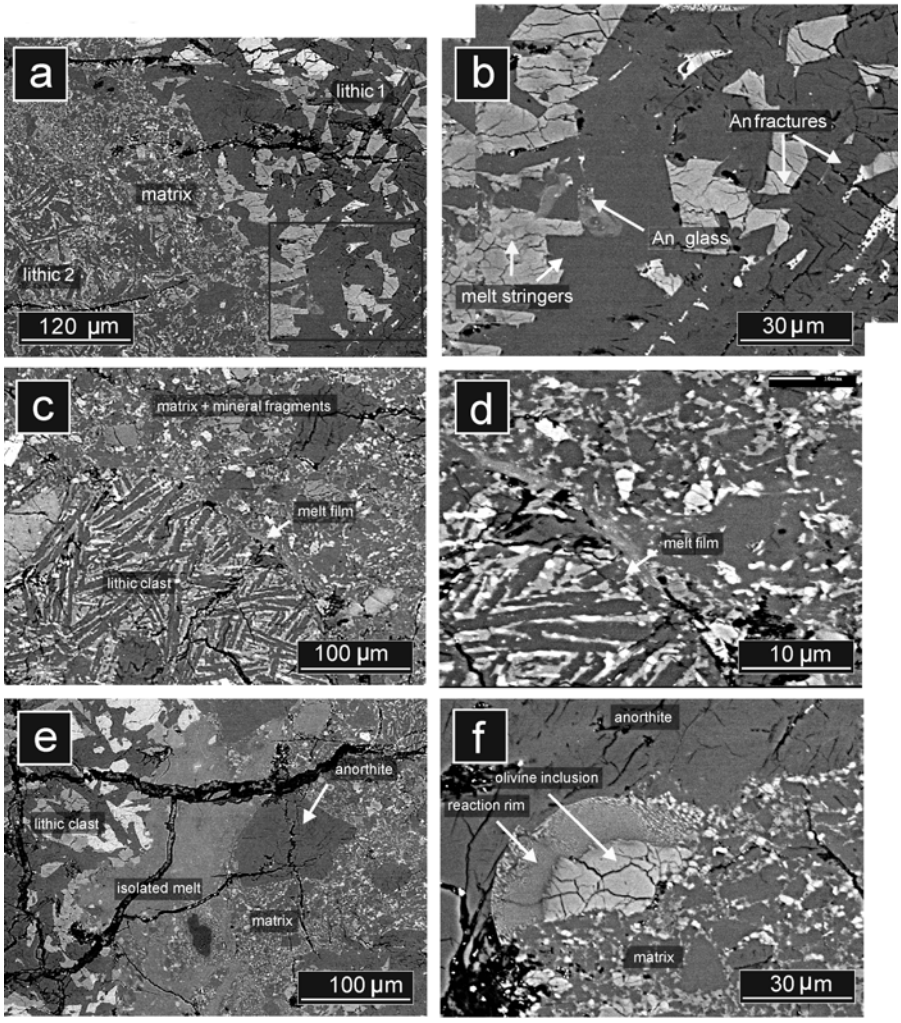

Fig. 2. BSE images of margins between matrix and lithic clasts. a) Overview of matrix-lithic clast relations. b) Close-up of area outlined in (a) showing isolated stringers and pockets of silicate melt near the clast margin. Anorthite, with irregular fractures and 1° birefringence throughout, has been transformed to glass near the matrix contact. Light areas are pyroxene grains. c) A thin film of melt occurs at a clast/matrix contact. d) Close-up of (c). e) An isolated pocket of silicate melt occurs at the margin between clast and matrix. f) Broken edge of lithic clast with olivine- (core) reaction rim inclusion set within anorthite host clast, juxtaposed with matrix.

to void space in the sample (fractures, vesicles, etc.); therefore, all totals between 90 and 100% were normalized for comparison. Melt pockets, veins, and lithic clasts were included in the bulk composition calculation. Ten raster scans of 170 × 120 µm areas of the matrix and nineteen scans representing five lithic clasts (170 × 120 µm areas) were also obtained. Owing to the small size and heterogeneity of the lithic clasts, there are inherent difficulties in determining their bulk compositions using conventional methods (e.g., INAA, XRF, etc.). These techniques involve crushing the sample as a whole, requiring the separation of the lithic clasts from the host rock. In addition, due to the rarity and value of lunar and meteoritic material, raster scan analysis is advantageous because it is nondestructive. The nondestructive nature, alkali mobilization minimization, and the ability to selectively raster single clasts make EDS raster scan analysis a viable method for estimating the bulk composition of individual clasts and the whole rock. We performed normative calculations using the CIPW program of Kurt Hollocher of Union College, Schenectady, New York, USA.

PETROGRAPHY

Photomicrographs and BSE images of the mineral assemblages of SaU 300 are shown in Figs. 1–6. The meteorite is a gray-colored crystalline-matrix breccia consisting of lithic and mineral clasts hosted by an aphanitic, dark gray matrix, all of which are crosscut by pockets of silicate melt material and veins. Both thin sections display several generations of fractures, some of which have been partly infilled by remobilized metal phases (<2 µm wide). We did not observe any regolith component (e.g., glass spherules, agglutinates) in either thin section.

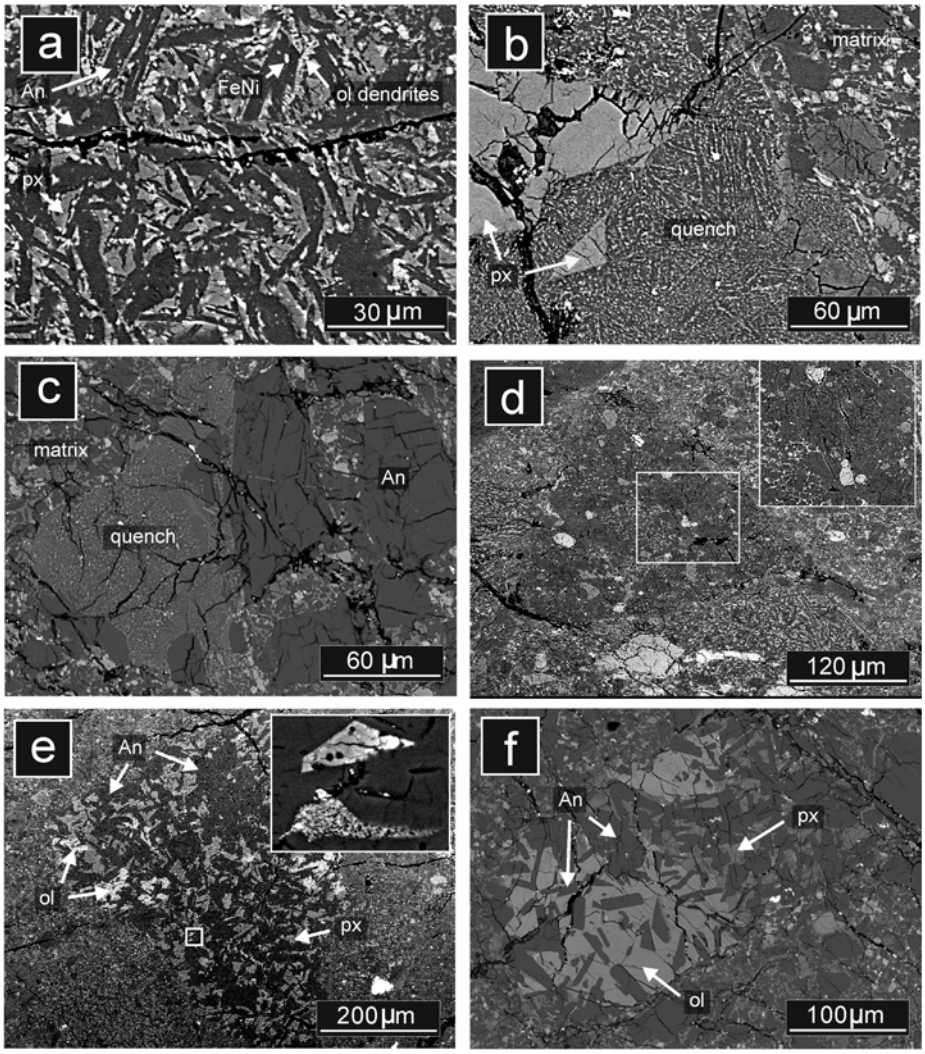

Fig. 3. BSE images of six impact melt clasts with distinct textures. a) Fine-grained (quench) impact melt texture. b) Glassy impact melt breccia clast showing a range in grain size from coarse, angular subclasts to fine-grained microcrystalline subclasts. c) Glassy impact melt breccia clast within coarse anorthite. d) A clast with an unusual texture of what appears to be an anorthositic impact melt breccia containing subangular clasts and pockets of impact melt enclosed by anorthite. e) One of the largest impact melt clasts observed in SaU 300, consisting of anorthite (An), pyroxene (px), and olivine (ol). Late-stage crystallization products, shown at higher magnification (inset), are silica, troilite, and Ti-rich pyroxene. f) An impact melt clast with a high proportion of mafics. Plagioclase laths are entirely (or almost entirely) isolated from one another.

ASEM reveals a fine-grained (defined here as all grains <10 µm), subophitic matrix consisting of mainly acicular plagioclase, pyroxene, and olivine, with minor ilmenite and FeNi (Fig. 1). The matrix is described in detail in the Mineral Composition section. We distinguished lithic clasts based on differences in texture, grain size, and mineral composition. Clasts range in size from 10 to 500 µm, although one anomalously large clast is 1200 µm. Lithic clast margins are smooth and appear to have been embayed and partially resorbed during their incorporation into the matrix (Figs. 2a–e). Clasts with sharp contacts are observed in places (Fig. 2f). The distribution of lithic clasts is variable on a centimeter scale. The lithic clast population of SaU 300 is dominated by impact-melt lithologies, with lesser proportions of metamorphic and granulitic clasts (Figs. 3 and 4). The lithic clast population (n = 34 for both thin sections) falls into the following categories: glassy impact-melt breccias (n = 15), crystalline impact-melt breccias (6), coarser-grained lithologies (12), and granulitic breccia (1).

Impact-Melt Clasts

The glassy impact-melt clasts are composed of thin (<10 µm) plagioclase laths and intersertal glass. Small grains of olivine (<5 µm) and olivine dendrites (Fig. 3a) have nucleated from the intersertal glass. We observed trace amounts of Fe metal blebs (<2 µm). Within this group, plagioclase and pyroxene grain sizes range from fine (quench-textured [<1 µm]) to moderately coarse-grained (50–100 µm) and they exhibit angular shapes (Figs. 3b and 3c).

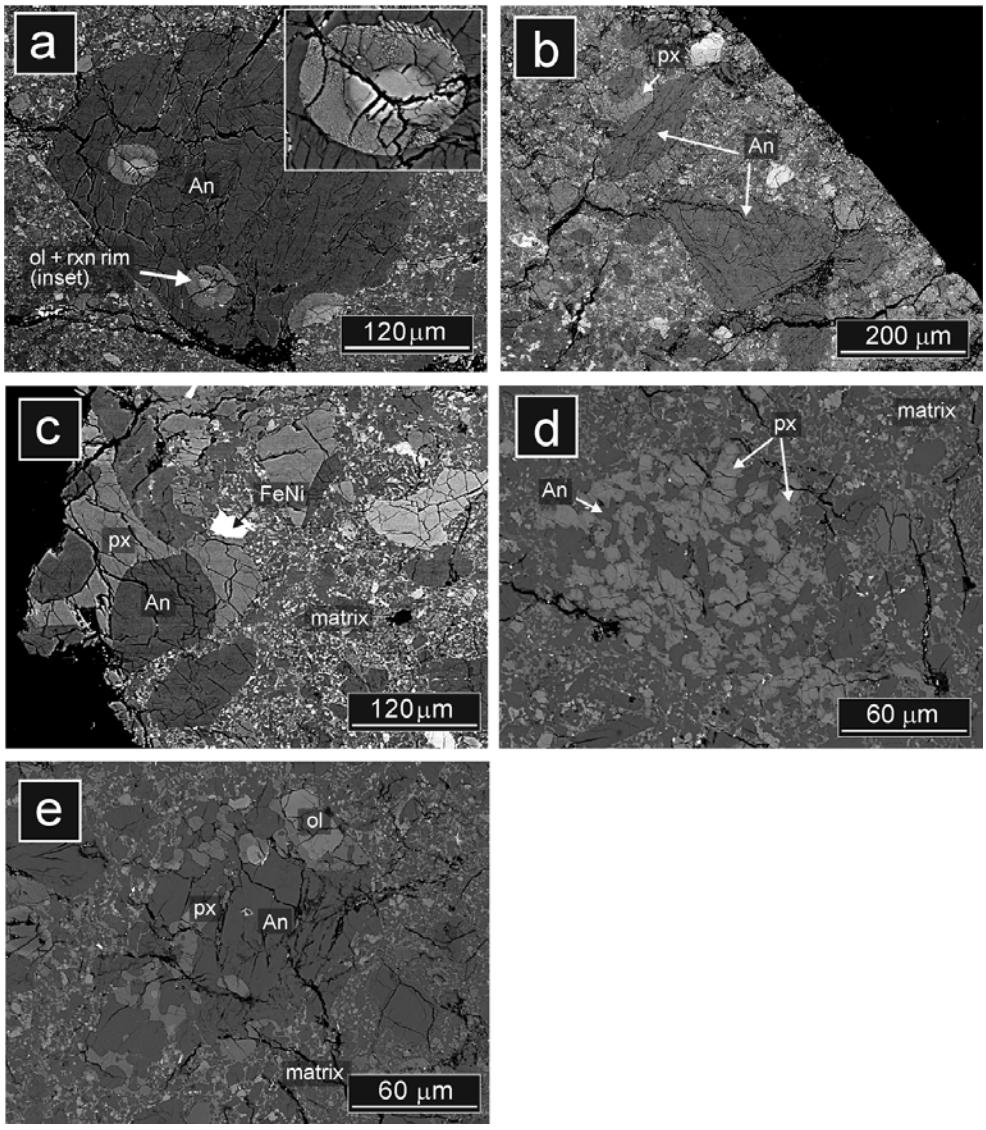

Fig 4. BSE images of four coarse-grained lithic clasts in SaU 300. a) Anorthite containing round inclusions of olivine (core) with a pyroxene-rich reaction rim. b) Clasts of predominantly anorthite with minor coarse pyroxene. c) Pyroxene enclosing subrounded anorthite. d) Zoned augite enclosing anorthite. e) Granulitic clast containing pyroxene, which poikilitically encloses anorthite and minor olivine. The clast exhibits homogeneous mineral compositions and a granulitic texture.

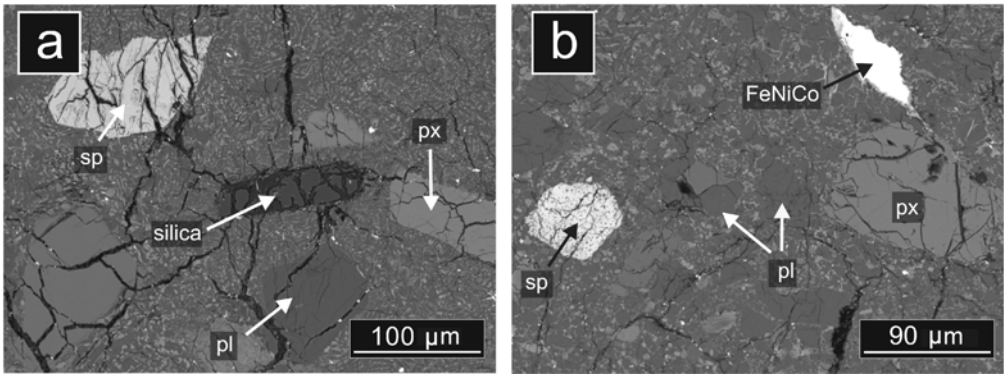

Fig. 5. BSE images of mineral fragments. a) Spinel (sp), silica, pyroxene (px), and plagioclase (pl) set within the very fine-grained crystalline matrix. b) As with (a), but with an FeNiCo fragment.

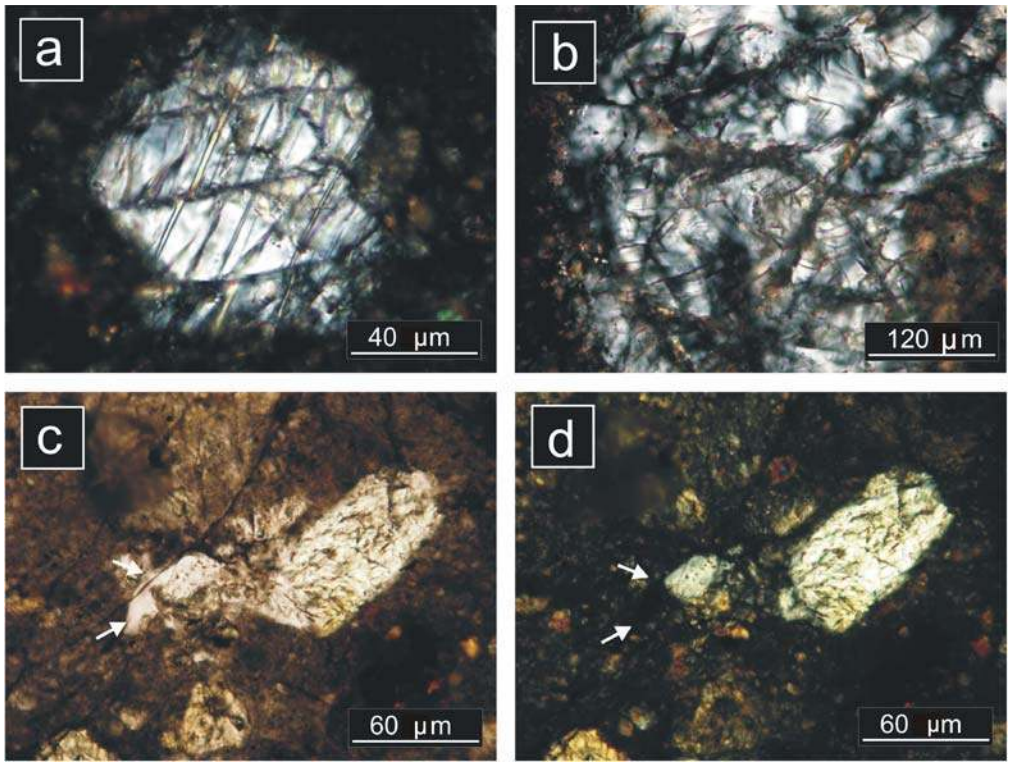

Fig. 6. Optical photomicrographs of SaU 300 anorthite in thin section. a) Anorthite mineral fragment showing mechanical deformation (offsetting of twin planes). b) Internally brecciated anorthite clast with patchy maskelynitization. c) Plane-light view of anorthite clast cut by shock vein (thin dark vein) as indicated by arrows. d) Cross-polarized image of (c). The anorthite devoid of fractures is optically isotropic.

One clast is anorthositic with Fe metal enclosed in the brecciated host grain (Fig. 3d). The interior of this clast contains pockets of probable glass.

The crystalline impact-melt breccias exhibit subophitic or poikilitic textures with plagioclase laths (100–200 μm) enclosed, or partially enclosed, by pyroxene (< 200 μm), with minor amounts of interstitial olivine (<100 μm) and metal. Late-stage assemblages have crystallized in the interstices to form an assemblage of high-Ti pyroxene, silica, and Fe sulfide (Fig. 3e).

Coarser-Grained Lithologies

The lithologies of the relatively coarse-grained clasts are difficult to determine with certainty because of their large grain size (30–120 μm) relative to clast size (100–1000 μm). At least five different lithologies are present. These clasts may be metamorphosed impact melts, possible plutonic lithologies (anorthosite, anorthositic norite), or recrystallized basaltic lithologies. All clasts exhibit rounded or resorbed edges. Textures range from granoblastic to poikilitic. Granoblastic clasts contain rounded plagioclase grains (<75 μm) with interstitial orthopyroxene (<50 μm) and olivine (<50 μm) (Fig. 4d). Poikilitic clasts contain subrounded plagioclase grains (50–150 μm) enclosed in pyroxene (<200 μm) and minor interstitial olivine (50 μm). Bartoschewitz et al. (unpublished data) describe lithic clasts of anorthositic olivine-gabbro, wehrlite, troctolite, and dunite, which we did not observe.

Granulitic Lithologies

We observed one clast of a granulitic lithology (Fig. 4e). The clast comprises granoblastic anorthite (<100 μm), which meets at triple junctions, and minor rounded olivine (<50 μm), all poikilitically enclosed in subrounded orthopyroxene (<200 μm). Anorthite commonly contains small (<10 μm), round inclusions of mafic minerals, mostly olivine, similar to the "necklace" grains observed in the Apollo granulitic breccias (Papike et al. 1998).

Mineral Fragments

Mineral fragments are dominated by anorthite, with lesser amounts of low-Ca pyroxene and olivine. Minor high-Ca pyroxene, ilmenite, Fe metal, chromite, and a silica phase are also present. Mineral fragment shapes are angular to subrounded and range in size from 10 to 700 μm (Fig. 5). It is considered likely that the mineral clasts were derived from breakdown of the lithic clasts, as their respective mineralogies are the same (see the Mineral Composition section).

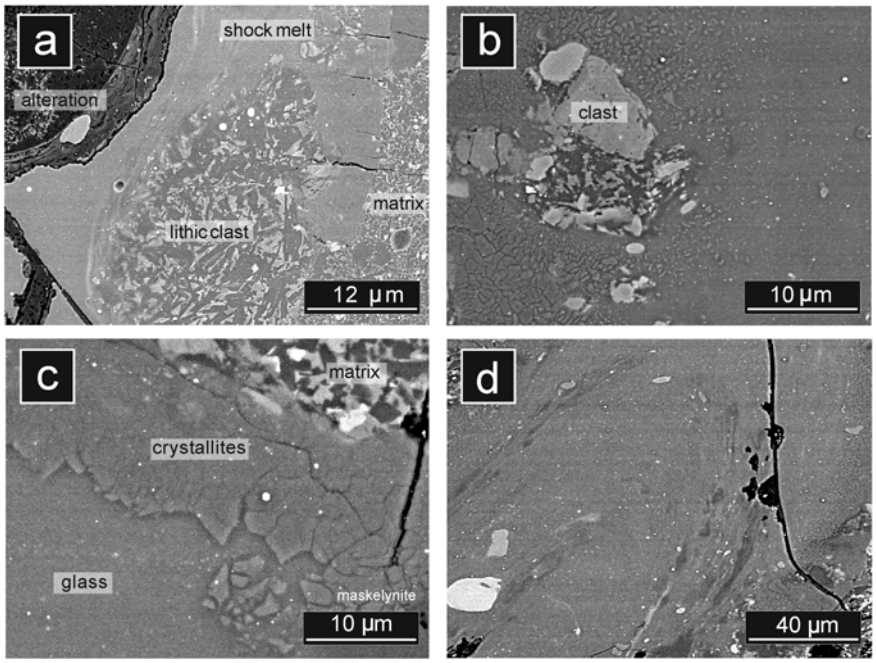

Fig. 7. BSE images of melt textures in SaU 300. a) Melt margin showing gradational boundary between schlieren-rich melt containing abundant spheres/blebs of Fe oxides and a lithic clast. b) A relatively cold clast entrained within the melt. c) Quench margin of the shock melt in contact with host rock. d) Schlieren-rich melt.

Shock Effects

The mineral and lithic clasts have been shocked to varying degrees (Fig. 6). In general, the coarser olivine fragments exhibit weak to moderate mosaicism and irregular or planar fractures. Up to two sets of planar fractures were observed in single grains. Smaller olivine grains exhibit undulose extinction. Pyroxene fragments exhibit weak to moderate mosaicism, curvature of cleavage or exsolution lamellae, displacement of exolution lamellae, and irregular or planar fractures (up to three sets in a single grain) (Fig. 6a). Plagioclase fragments show a wide variety of shock effects, including undulose extinction, mechanical deformation, and kink bands, in addition to local transformation to maskelynite in areas adjacent to localized melt features (veins and pockets) (Figs. 6b and 6c). Severely fractured grains (mineral and lithic) show internal brecciation (Fig. 6d).

Localized shock melts cut across the host rock and form two distinct features:

- thin (10–300 µm) melt veins that offset and shear neighboring minerals, and
- irregularly shaped pockets (mm size) of silicate melt with melt veins emanating from their margins (Fig. 7).

Isolated pockets of glass or glass rinds may occur at the contacts of clasts and matrix (Fig. 2e).

In plane light, melt pockets have dark brown rims and light brown interiors. BSE investigation reveals a glassy, schlieren-rich internal texture containing abundant blebs of sulfides and Fe metal, as well as rounded clasts of locally derived host rock that were partially digested during incorporation into the melt (Figs. 7a and 7b). The contact with the host rock clasts is characterized by a 10–40 µm (apparent diameter) chill zone of fine-grained crystallites, which radiate into the melt pocket groundmass (Fig. 7c). We interpret the crystallites to have formed by quenching due to contact with the relatively cold host rock. They are probably not devitrification features, which would show a relationship to any free surface (e.g., open fractures that cut across the melt pockets) (Lofgren 1980). Melt vein textures are similarly dominated by schlieren-rich glasses containing spheres of immiscible sulfides and oxides, and rounded mineral fragments (Fig. 7d).

The thin sections are cut by partially infilled fractures that crosscut the melt pockets and veins. These are filled with gypsum and Ca carbonates, presumably formed during the meteorite's residence in a terrestrial hot desert environment. Local fracture systems also extend from the quench margins of the pockets into the host rock, but are limited to a few tens of microns from the melt/host rock contact. These fractures are not pervasive and were probably formed by volume expansion and contraction associated with melting and crystallization of pockets and veins.

Mineral and Glass Compositions

Matrix

Compositional ranges of representative matrix minerals are given in Table 1. The matrix of SaU 300 consists of

Table 1. Compositional ranges of representative matrix minerals and mineral fragments in SaU 300, based on EDS analysis.

Phase	Size range	Compositional range
Matrix		
Plagioclase	<10 μm	$An_{94–98}$
High-Ca px	<10 μm	$Wo_{37}En_{44}$–$Wo_{39}En_{47}$
Pgt	<10 μm	Wo_8En_{69}
Low-Ca px	<10 μm	Wo_4En_{65}–Wo_4En_{75}
Ol	<10 μm	$Fo_{62–72}$
Mineral fragments		
Plagioclase	10–700 μm	$An_{93–96}$
High-Ca px	10–500 μm	$Wo_{18}En_{30}$ –$Wo_{43}En_{48}$
Pgt	10–250 μm	Wo_7En_{67}–$Wo_{14}En_{44}$
Low-Ca px	10–500 μm	Wo_4En_{77}–Wo_5En_{70}
Ol zoned–core	n.a.	$Fo_{67–91}$
Ol zoned–rim	n.a.	$Fo_{62–71}$
Ol unzoned	10–700 μm	$Fo_{63–73}$

acicular anorthite needles ($An_{94–98}$) with interstitial euhedral orthopyroxene ($Wo_4En_{65–76}Fs_{21–31}$), clinopyroxene ($Wo_{37–39}En_{44–47}Fs_{14–19}$), and minor olivine ($Fo_{62–72}$), as well as a minor amount of irregularly shaped Fe metal and ilmenite grains. Only one grain of pigeonite was observed in the matrix ($Wo_8En_{69}Fs_{23}$).

Mineral Fragments

Plagioclase Clasts: Compositional ranges and representative mineral analyses are given in Tables 1 and 2, respectively. Plagioclase is anorthite with a small compositional range ($An_{93–96}$; average An_{95}). Plagioclase always contains FeO (0.1–1.2 wt%) and MgO (0.1–0.9 wt%). In general, plagioclase from the matrix ($An_{94–98}$) and mineral fragments ($An_{93–96}$) (Fig. 8a) exhibit the same compositional range as lithic clasts ($An_{93–97}$; Tables 1 and 2). A few anorthite grains contain small, rounded, necklace-like inclusions of olivine having a composition of Fo_{75}.

Olivine Clasts: The compositions of pyroxene and olivine are variable, as summarized in Table 1. Typically, olivine mineral fragments are zoned from Mg-rich cores ($Fo_{67–91}$) to thin (a few microns), more ferroan rims ($Fo_{63–72}$). Two main compositional groups were observed: 1) more common Mg-rich ($Fo_{61–91}$) unzoned mineral clasts, and 2) more ferroan ($Fo_{45–56}$) zoned and unzoned mineral clasts, matrix grains, and grains in lithic clasts (Fig. 8b). All olivine is rich in Cr (up to 0.49 wt% Cr_2O_3).

Pyroxene Clasts: Both high-Ca and low-Ca pyroxene mineral clasts are present, with pigeonite occurring in greater proportions. Some grains exhibit gradual zoning from $Wo_{10–20}En_{50–63}Fs_{22–38}$ (core) to $Wo_{4–9}En_{48–64}Fs_{28–51}$ (rim). A few larger pigeonite grains exhibit micrometer-thick lamellae, which are too thin for quantitative analysis. High-Ca pyroxene mineral fragments exhibit a wide range of compositions ($Wo_{18–43}En_{30–49}Fs_{9–52}$ and Mg# 42–85). Pigeonite mineral fragments also exhibit a large range of compositions ($Wo_{7–14}En_{44–67}Fs_{27–42}$ and Mg# 51–71) (Fig. 9). Pyroxenes with less than Wo_5 are rare. Orthopyroxene mineral fragments range in composition from $Wo_{4–5}En_{70–77}Fs_{19–24}$ (Mg# 74–80). In general, pyroxene compositions of lithic clasts overlap with those analyzed from mineral fragments and the matrix (Table 3).

Based on the two-pyroxene thermometer of Lindsley and Anderson (1983), the sample last equilibrated at 1000–1200 °C (Fig. 9). Pyroxenes in the matrix, lithic clasts, and mineral clasts all fall within this range, indicating that the clasts re-equilibrated during juxtaposition with the hot melt sheet, or that they exhibit similar equilibration temperatures due to previous separate heating events.

Minor Phases: Representative ASEM and EMP data for minor phases are summarized in Table 4. Of the minor mineral constituents, Fe metal is the most abundant. It occurs as grains in the matrix, in lithic clasts, and is sparsely dispersed as metallic iron alteration products in cavities and fractures. Metal grains are typically small (2–100 μm), with Ni concentrations ranging from 1.1 to 9.7 wt% and Co concentrations from 0.6 to 1.5 wt%. Metal grains exhibit low Co contents for a given Ni content (Fig. 10), indicating an exogenous or meteoritic origin. Spinels are Cr-rich (39.0–46.5 wt%) and occur only as mineral clasts (75–100 μm). One spinel grain contains 0.11 wt% ZrO_2 and 0.09 wt% NiO. Ilmenite occurs as small (<50 μm) mineral fragments, matrix grains, and fills fractures in the larger mineral clasts. It is rich in MgO (up to 6.4 wt%).

Mineral clasts of armalcolite, spinel proper, ulvöspinel, and trace troilite were identified by Bartoschewitz et al. (unpublished data), but were not observed as mineral fragments in the thin sections investigated in this study. However, armalcolite and troilite were identified as minor phases in certain lithic clast types (see the following section).

Lithic Clasts

Compositional ranges and representative analyses of lithic clasts are given in Tables 2 and 3, respectively. Classification was determined by modal analysis of the clasts using the definitions of Stöffler et al. (1980). Small clast sizes may bias the modal classifications. Most lithic clasts are anorthositic and have variable plagioclase to mafic mineral ratios. Five clasts were rastered. All are more ferroan than the matrix composition (Mg# 56–65 for clasts and 67 for the matrix) (Fig. 11). In lithic clasts, pyroxene and olivine grains exhibit a wide range of compositions. Mg#s range from 53 to 75 for olivine grains and between 23 and 84 for pyroxene grains (average 60). The wide range of compositions indicates a number of distinct sources for these lithic clasts.

Table 2. Compositional ranges of representative lithic clasts in SaU 300.

Clast	Dimension (mm)	Textures	Pyroxene	Plagioclase	Olivine	Accessory mineralogy
Glassy impact melts						
2	0.4 × 0.5	Subophitic	Wo_9En_{66}	$An_{95–96}$	Fo_{53}	FeNi metal
6	0.4 × 0.6	Subophitic	$Wo_{47}En_{34}$–$Wo_{56}En_{29}$	$An_{93–96}$	n.a.	FeNi metal, large entrained pgt (Wo_8En_{61})
O	0.2 × 0.1	Pilotaxitic	n.a.	$An_{94–95}$	n.a.	FeNi metal in fractures
Clastic impact melts						
1	1.4 × 0.8	Subophitic	Wo_2En_{70}–$Wo_{12}En_{58}$	$An_{93–96}$	$Fo_{60–63}$	FeS, silica, and high-Ti px
4	0.3 × 0.3	Variable/ brecciated	Wo_2En_{70}	$An_{95–96}$	Fo_{66}	Armalcolite
J	0.3 × 0.2	Poikilitic	$Wo_{11}En_{60}$–$Wo_{12}En_{60}$	An_{96}	Fo_{61-66}	FeNi metal
N	0.1 × 0.1	Subophitic/ poikilitic	n.a.	An_{97}	Fo_{66}	FeS or FeNi metal
A	Unknown	Subophitic	$Wo_{24}En_{33}$	An_{96}	n.a.	n.a.
Granulitic lithologies						
H	0.2 × 0.1	Granoblastic	$Wo_{10}En_{66}$	An_{96}	$Fo_{66–69}$	n.a.
Coarser grained lithologies						
3	0.4 × 0.5	Unknown	$Wo_{28–31}En_{48–50}Fs_{22–23}$	An_{95}	$Fo_{73–85}$	Round inclusions with ol core and px rim
5	Unknown	Poikiloblastic	Wo_4En_{75}	An_{95}	n.a.	n.a.
D	0.2 × 0.2	Cumulate	Wo_3En_{71}	An_{95}	Fo_{68}	FeNi metal or FeS
F	0.4 × 0.2	Cumulate	$Wo_{24–31}En_{18–48}Fs_{23–58}$	An_{96}	n.a.	n.a.
G	0.2 × 0.1	Poikiloblastic	$Wo_{10}En_{60}$	An_{94}	Fo_{54}	FeNi metal
I	0.2 × 0.1	Cumulate	$Wo_{15}En_{47}$	An_{94}	n.a.	Minor FeNi metal
K	1.3 × 0.7	Granulitic	n.a.	$An_{95–96}$	n.a.	FeNi metal or FeS in fractures
M	0.4 × 0.3	Poikilitic	?	An_{95}	Fo_{64}	n.a.

Based on EDS and WDS analysis. Clasts with unknown dimensions are truncated by the thin section edge. Mineralogy refers to minor mineral phases in the lithic clasts. Numerical and alphabetical references to clast type are illustrated in Figs. 3 and 4.

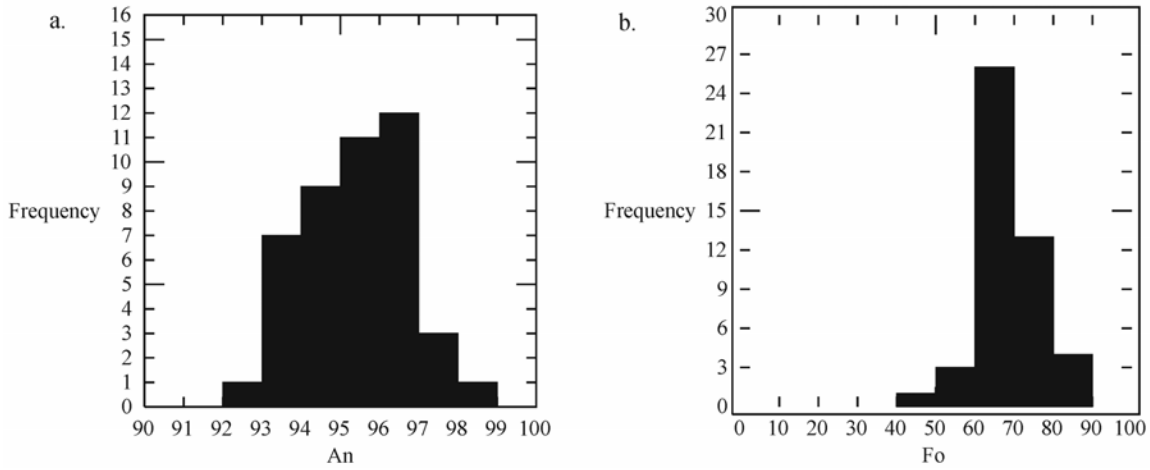

Fig. 8. Compositions of plagioclase and olivine in SaU 300. Boxes are for matrix minerals and mineral fragments. a) Anorthite content of plagioclase in SaU 300. $N = 44$; mean = 95.3; std. dev. = 1.2. b) Forsterite content of olivine (atomic Mg/[Mg + Fe]) $N = 47$; mean = 67.4; std. dev. = 8.1.

Impact-Melt Clasts: Glassy impact-melt clasts contain acicular plagioclase ($An_{95–96}$) with interstitial, zoned orthopyroxene and pigeonite ($Wo_{2–10}En_{50–70}Fs_{26–32}$) in addition to minor olivine ($Fo_{53–62}$), troilite, and low-Ni Fe metal. One large clast (400 μm) of glassy impact melt contains a large (250 μm) clast of pigeonite ($Wo_8En_{31}Fs_{61}$). The melt matrix of this clast exhibits a quench texture of fine-grained, acicular anorthite ($An_{93–96}$), clinopyroxene ($Wo_{47–49}En_{29–34}Fs_{15–20}$), and minor blebs of FeNi metal (<2 μm).

Clastic impact-melt clasts contain acicular plagioclase ($An_{93–97}$) enclosed in zoned pyroxene ($Wo_9En_{53}Fs_{38}$–$Wo_{11}En_{63}Fs_{26}$) with minor olivine ($Fo_{60–66}$), troilite, and Fe metal.

Table 3. Representative ASEM and EMP data for major phases in SaU 300.

	Mineral fragments						Lithic clasts						Matrix				
					Olivine		plag	aug	aug	pgt	opx	ol					
wt%	plag	aug	pgt	opx	core	rim	C1	C3	C3	C1	C5	C4	plag	cpx	pgt	opx	ol
SiO_2	44.2	50.9	53.3	54.8	38.4	37.0	44.4	47.2	40.9	51.5	53.8	36.1	44.2	50.6	53.9	53.4	36.8
TiO_2	0.1	0.3	0.5	1.0	b.d.	0.2	0.0	3.4	0.0	0.7	0.9	0.0	b.d.	2.2	0.6	0.6	0.2
Al_2O_3	35.9	1.5	1.1	1.5	0.2	0.5	34.9	3.1	21.4	1.3	1.3	0.0	35.3	2.5	1.9	1.6	0.4
Cr_2O_3	0.2	0.7	0.4	0.6	0.3	0.4	b.d.	0.5	0.1	0.6	0.5	0.0	b.d.	b.d.	0.6	b.d.	0.2
FeO	0.1	23.3	20.6	12.5	22.4	30.4	1.2	21.0	11.3	20.3	14.4	30.7	0.5	11.4	14.0	14.1	29.9
MnO	b.d.	0.4	b.d.	0.0	0.3	0.4	0.0	0.4	0.2	0.4	0.3	0.3	0.2	0.4	b.d.	0.4	0.5
MgO	0.3	13.3	19.1	27.8	38.1	30.5	0.6	10.8	13.2	21.1	27.4	33.3	0.5	15.1	23.9	26.9	31.1
CaO	19.2	9.0	4.3	1.8	0.1	0.7	18.4	13.9	12.1	4.2	1.9	0.2	19.4	17.8	3.9	2.1	0.4
Na_2O	0.4	0.2	0.2	0.2	0.3	0.3	0.5	0.1	0.2	0.1	0.0	0.0	0.3	0.4	0.3	0.3	b.d.
K_2O	0.1	0.1	b.d.	b.d.	0.1	0.2	0.1	0.0	0.0	b.d.	b.d.	b.d.	0.1	0.1	b.d.	0.1	b.d.
Total	100.3	99.6	99.5	100.3	100.3	100.7	100.0	100.3	99.4	100.2	100.5	100.8	100.6	100.8	99.1	99.8	99.6
An/Wo/Fo	96	20	9	4	75	64	95	31	31	9	4	66	97	37	8	4	65
Ab/En/Fa	4	41	57	77	25	36	5	33	47	59	74	34	3	44	69	74	35
Or/Fs	0	40	34	19			0	36	23	32	22		0	19	23	22	
Mg#	100	51	62	80	75	64	46	48	67	66	71	66	63	70	75	77	65

C1 = clast 1 (impact melt); C3 = clast 3 (impact melt); C4 = clast 4 (impact melt); C5 = clast 5 (coarse-grained lithology). b.d. = analyses below detection limits.

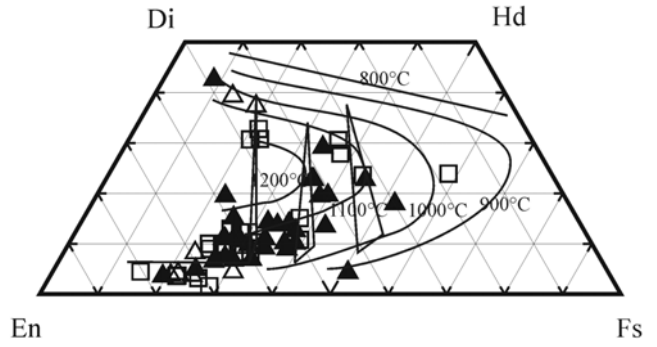

Fig. 9. Pyroxene quadrilateral compositions for SaU 300 superimposed on the two-pyroxene thermometer of Lindsley and Anderson (1983). Open triangles = matrix px; closed triangles = px fragment; open squares = lithic clasts. Pyroxenes both follow and lie between the 1000 °C and 1200 °C isotherms. Matrix compositions mostly lie along the 1100 °C isotherm.

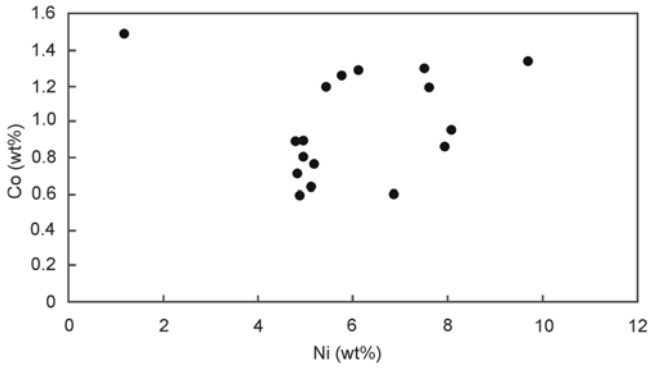

Fig. 10. Variation in cobalt and nickel composition among native iron metal grains in SaU 300. Most analyzed grains fall within the range of meteoritic metal as defined by Hewins and Goldstein (1975). This composition is common in lunar feldspathic impact melt rocks (Papike et al. 1998).

The 350 μm clast of anorthositic impact breccia contains subangular grains of olivine (Fo_{66}) and orthopyroxene ($Wo_2En_{29}Fs_{70}$) and minor amounts of armalcolite and FeNi metal in a host grain of brecciated anorthite ($An_{95–96}$).

Coarser-Grained Lithologies: Coarser-grained lithic clasts include:

1. Clasts that contain orthopyroxene ($Wo_4En_{22}Fs_{75}$) enclosing anorthite (An_{95}) and minor ilmenite with a gabbroic anorthosite bulk composition.
2. Anorthositic clasts composed almost entirely of anorthite ($An_{94–97}$) with minor zoned clinopyroxene ($Wo_{30}En_{48}Fs_{22}$ to $Wo_{24}En_{47}Fs_{29}$), rounded olivine (Fo_{76}), and Fe metal grains.
3. Fragments containing ~60% plagioclase (An_{96}), ~30% orthopyroxene ($Wo_3En_{47}Fs_{50}$), and ~10% olivine (Fo_{68}) with a bulk composition of anorthositic norite.

Table 4. Representative ASEM and EMP data for minor phases in SaU 300.

	Matrix		Mineral clasts			Clast 1
wt%	Ilm	FeNi	Spinel	FeNi	Si-phase	Mg Ilm
SiO_2	0.5	0.2	0.3	0.2	99.0	0.0
TiO_2	54.1	b.d.	10.0	b.d.	0.2	55.5
Al_2O_3	0.6	0.1	12.0	0.1	0.5	0.0
Cr_2O_3	1.4	b.d.	39.0	b.d.	0.3	0.5
FeO	35.0	90.4	30.7	94.2	0.4	36.6
MnO	0.2	0.0	0.3	0.0	0.2	0.3
MgO	5.3	0.1	6.2	0.2	b.d.	7.2
CaO	0.9	0.3	0.3	0.4	0.1	0.1
Na_2O	b.d.	b.d.	0.2	b.d.	b.d.	b.d.
Co	1.8	0.9	b.d.	0.8	0.2	n.a.
Ni	b.d.	7.9	0.4	5.1	0.1	n.a.
Total	99.8	99.8	99.5	100.9	101.0	100.3

Ilm = ilmenite; FeNi = iron-nickel metal; Mineral clast = monomineralic mineral fragment; Mg Ilm = magnesian ilmenite.
n.a. = element was not analyzed.
b.d. = below detection limits.

4. Fragments containing coarse intergrowths of plagioclase ($An_{94–97}$) and olivine ($Fo_{60–67}$), with a bulk composition of troctolitic anorthosite, and 5 clasts containing zoned augite oikocrysts ($Wo_{15}En_{48}Fs_{37}$) enclosing anhedral anorthite crystals (An_{94}) with a gabbroic composition.

One clast of anorthite (Fig. 4a) consists of anorthite (An_{95}) containing round inclusions of olivine ($Fo_{73–85}$) with a reaction rim of composition $Wo_{28–31}En_{47–50}Fs_{22–23}$, as determined by defocused beam analysis. These coarser-grained clasts may represent metamorphosed impact melts, metamorphosed basalts, or possible plutonic lithologies. Due to small clast sizes, lithologies were difficult to determine with certainty.

Granulitic Lithologies: The granulitic clast contains granoblastic anorthite ($An_{93–96}$) enclosed by pyroxene oikocrysts ($Wo_{10}En_{60–66}Fs_{24–30}$) and olivine mineral fragments ($Fo_{54–66}$). As with the Apollo granulites, mineral compositions are homogenous throughout the clast.

Melt Pockets and Shock Veins

Representative compositions of shock glasses from SaU 300 are given in Table 5. The compositions of melt pockets and veins are indistinguishable from one another, but exhibit a wide range (Fig. 11). The majority of analyses are highly feldspathic (>28 wt% Al_2O_3) or moderately feldspathic (22–28 wt% Al_2O_3), but there is a small group of moderately mafic (15 wt% FeO) to highly mafic (26–27 wt% FeO) glasses. All the melts have very low concentrations of TiO_2 (<0.6 wt%). The most mafic clasts exhibit the lowest concentrations (0.01–0.05 wt% TiO_2). Individual analyses with elevated NiO (0.1–0.2 wt%) and S (0.2–0.5 wt%) reflect areas of melt that contain spheres and blebs of immiscible sulfides and metallic iron. Small (1–2 μm) rounded metal

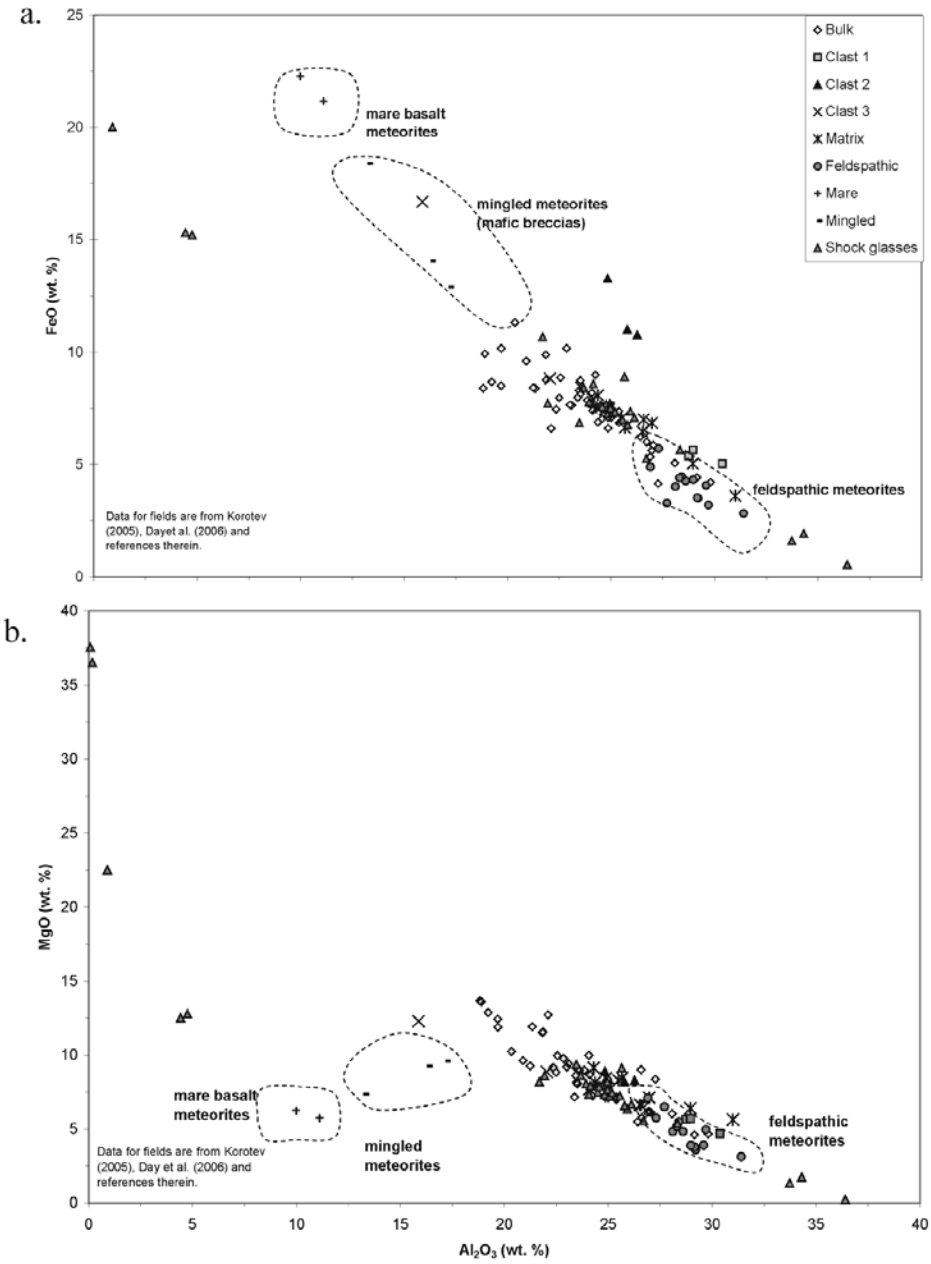

Fig. 11. Plot of Al_2O_3 (in weight percent) versus (a) FeO and (b) MgO. Included are whole rock, matrix, lithic clast, glass, and shock melt compositions for SaU 300. These have been plotted against the compositions of a range of other meteorites taken from the literature (data from Korotev [2005], Day et al. [2006] and references therein).

grains have been remobilized and distributed in fractures throughout the meteorite.

Weathering Products

Compositional and crystallographic data were not collected from the weathering products, but they appear to be dominated by Ca carbonate, gypsum, minor sulfates, and metallic iron alteration products (most likely hematite and goethite), based on EMP analysis and EDS spectra. Larger FeNi metal grains (20–100 μm) are present as clasts throughout the matrix, and possess a thin rust-colored rim but are otherwise internally intact. A rusty orange-brown staining is visible in many areas of SaU 300 and is especially notable both near the shock melts and in cracks and fractures of olivine mineral clasts. The weathering scale of Wlotzka (1993) was developed for ordinary chondrites, but is based on petrographic criteria that can be applied to SaU 300. The petrographic features observed in this study indicate a weathering grade of W1.

BULK COMPOSITION

Raster scan analyses of the thin sections (matrix plus clasts) indicate that SaU 300 is a plagioclase-rich rock (68%) with a bulk composition of olivine-rich anorthositic norite. With an average bulk Al_2O_3 content of 24 wt%, SaU 300 falls between the compositions of anorthositic (25–35 wt%) and basaltic (8–12 wt%) lunar rocks, indicating that it may comprise a mixture of the two lithologies, with a preferential incorporation of anorthositic material. Minerals from the lithic clasts in SaU 300 plot between the ferroan anorthosite and magnesian suite fields (Fig. 12), and within the magnesian granulitic breccia field on the (Th/Sm) CI-normalized graph of Korotev (2005). Bartoschewitz et al. (unpublished data) report values for Th (0.5 ppm), Sc (18.0–22.0 ppm), and Sm (1.1 ppm). SaU 300 is one of the most siderophile element-rich lunar meteorites studied to date. Based on our analysis and data obtained from Bartoschewitz et al. (unpublished data), SaU 300 is rich in Ni (0.08 wt%), Co (0.073 ppm), Ir (0.042 ppm), and Au (0.047 ppm) relative to chondrites, as a result of the presence of a meteoritic component. (Co, Ir, and Au were analyzed via ICMP, TXRF, and INAA, as reported in Bartoschewitz et al. [unpublished data]).

Most analyzed clasts were more ferroan than the matrix (Mg# 56–65 versus 67 for the matrix). The matrix is more calcic than most clasts. The matrix of SaU 300 contains more Al_2O_3 than the bulk rock (27 wt% versus 24 wt%) and is normatively a troctolitic anorthosite (Fig. 11). The bulk Al_2O_3 content (average 24 wt%) falls within the range of the values determined by conventional techniques (ICPMS: 20.4–24.1 wt%) (Bartoschewitz et al., unpublished data), which supports the application of raster scanning as an alternative, nondestructive method of estimating bulk composition for lunar samples, meteorites, and other rare materials. The FeO content of the bulk rock is high (~8 wt%) compared to the other analyzed feldspathic meteorites. If classified according to the fields of Korotev (2005) (Fig. 11), SaU 300 extends in the lunar feldspathic meteorite field. That is, it is the most mafic of the feldspathic lunar meteorites. The bulk of SaU 300 is rich in TiO_2 (up to 0.5 wt% in the matrix) compared to the other feldspathic meteorites; most feldspathic meteorites contain 0.2–0.3 wt% TiO_2. Since SaU 300 is richer in FeO, and TiO_2 content is correlated with FeO content, it is expected to be richer in TiO_2 without requiring the incorporation of a basaltic component (see Korotev 2005). However, there is no definitive evidence for the presence of lithic clasts of mare basalt.

DISCUSSION

Provenance

The relatively coarse-grained textures of the lithic clasts incorporated into the matrix indicate that SaU 300 originated from a differentiated parent body. Four main lines of evidence support a lunar origin:

Table 5. Representative analyses of shock melts in SaU 300.

	Shock glasses			
	Melt pocket		Veins	
	feld	mafic	feld	mafic
SiO_2	43.9	36.4	44.5	37.1
TiO_2	0.3	b.d.	0.3	0.1
Al_2O_3	24.1	0.2	23.4	0.1
Cr_2O_3	0.2	0.3	0.2	0.1
FeO	8.6	26.2	8.3	26.3
MnO	0.1	0.3	0.1	0.3
MgO	7.9	36.2	8.6	36.5
CaO	14.2	0.5	14.1	0.1
Na_2O	0.3	0.0	0.4	0.0
K_2O	0.1	b.d.	0.1	b.d.
P_2O_5	0.0	0.1	0.1	b.d.
SO_3	0.4	0.1	0.4	b.d.
Ni	0.1	b.d.	b.d.	b.d.
Co	0.0	0.1	0.0	0.0
Total	100.3	100.3	100.3	100.5

feld = feldspathic glass compositions.
mafic = mafic glass compositions.

1. A high anorthite content in plagioclase (average An_{95}).
2. A high chromium content in olivine (up to 0.49 wt% Cr_2O_3).
3. A lack of hydrous minerals.
4. Textural, mineralogical, and chemical similarities to the Apollo samples.

Terrestrial anorthosites are uncommon and most have anorthite contents in the range of 40–80, with the exception of rare Archean anorthosites, which have anorthite contents of up to An_{90} (Ashwal 1998). Terrestrial olivines do not typically contain high amounts of Cr, because Cr^{3+}, the normal valance state for Cr in terrestrial olivines, is not as readily accommodated into the olivine structure as Cr^{2+}, the normal valance state of Cr on the Moon (Papike et al. 1998).

The Fe/Mn ratio of bulk rock and/or mafic mineral compositions is a commonly used indicator of planetary origin (Papike et al. 1998). The Fe/Mn ratios of pyroxene and olivine in SaU 300 lie approximately along the lunar line (Fig. 13), although the range of values is too large to be conclusive (pyroxenes average 63 ± 12, and olivines average 99 ± 13). Ratios do not vary between clasts and matrix, but the spread of numbers is large (46–84 for pyroxene and 82–116 for olivine). However, this spread is typical for lunar olivines and pyroxenes, and ratios for SaU 300 are bracketed by the range of values seen in other lunar rocks (65–160 for olivine and 32–84 for pyroxene) (Papike et al. 1998). The Fe/Mn ratios of pyroxenes and olivines in Apollo samples average about 70. Fe/Mn ratios for terrestrial pyroxenes average about 45 and about 75 for olivines (Papike et al. 1998).

SaU 300 has been previously classified as a lunar anorthositic highland regolith breccia with basaltic and granulitic components (Bartoschewitz et al., unpublished

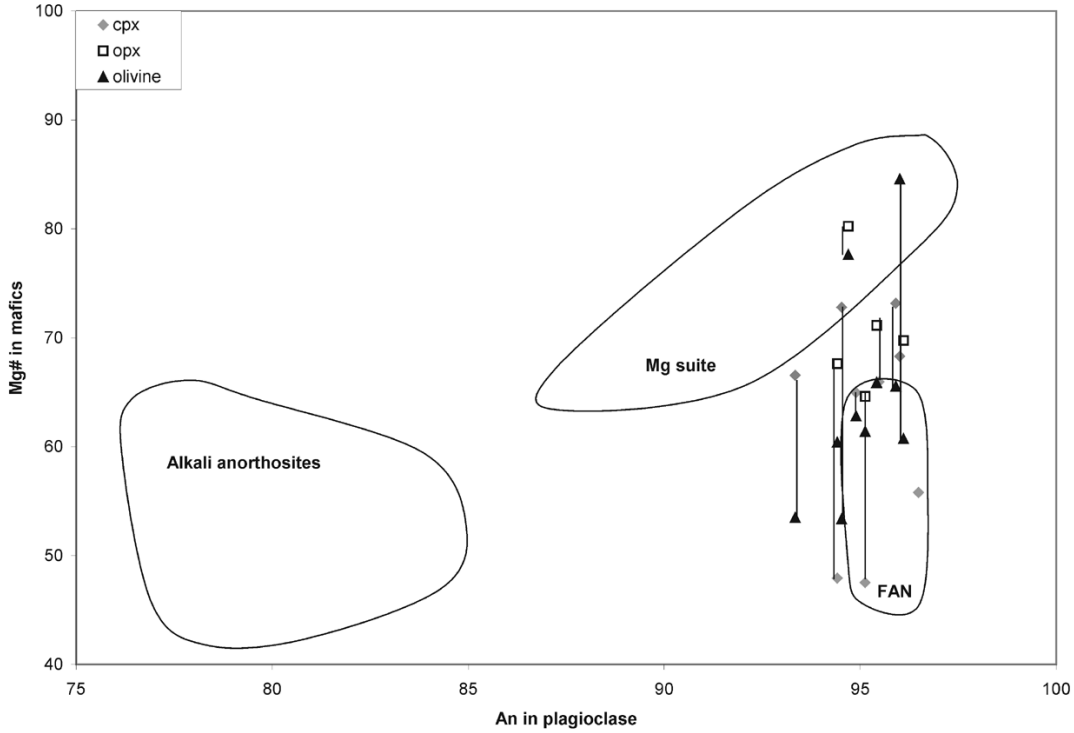

Fig. 12. Mg# (molar Mg/[Mg + Fe] × 100) in mafic minerals (olivine and pyroxene) versus An (molar Ca/[Ca + Na + K] × 100) in feldspars for minerals present in the lithic clasts observed in SaU 300. Fields are for the pristine rock suites (Warren et al. 1983). FAN = ferroan anorthosite suite.

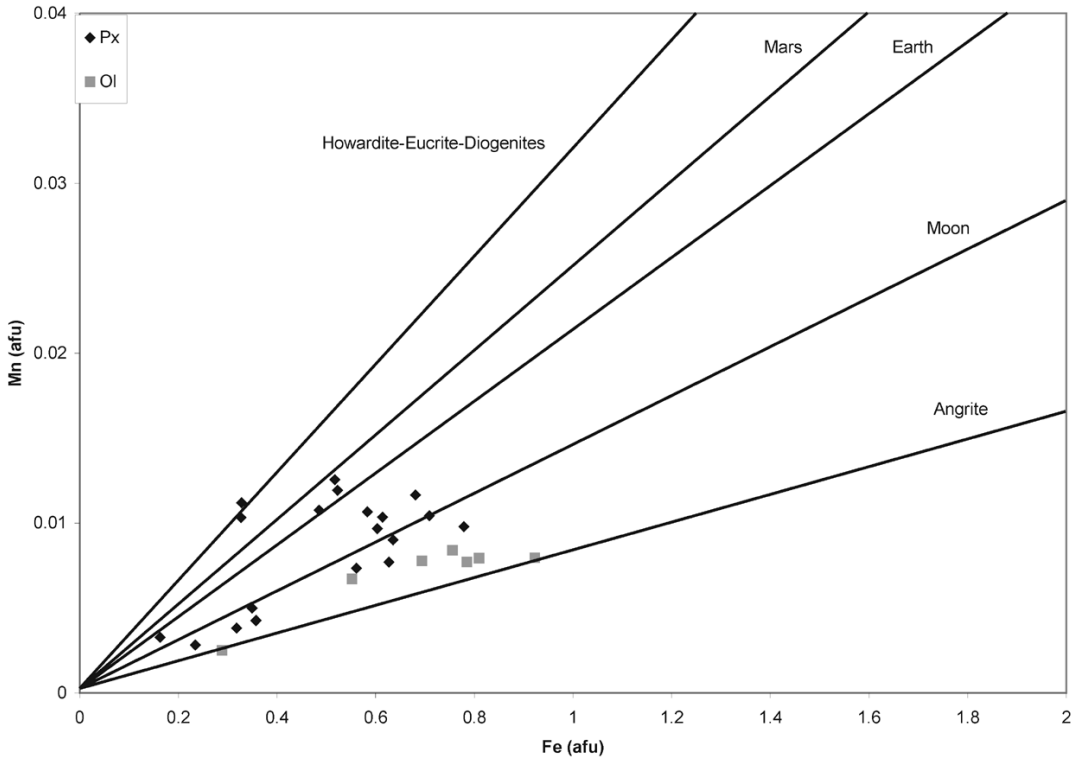

Fig. 13. Plot of Fe versus Mn (in atomic formula units) for SaU 300. Fe/Mn ratios support a lunar origin for this meteorite. Planetary heritage lines are from Papike et al. (1998). Data from WDS analysis.

data). Noble gas isotopes, as reported by Bartoschewitz et al. (unpublished data), are poor in solar wind components, interpreted in their abstract as indicating the loss of noble gases by thermal metamorphism at ~1200 °C giving rise to a granulitic texture. However, save for one granulitic lithic clast, we see no textural or compositional evidence that SaU 300 has undergone bulk thermal annealing (i.e., no triple point junctions, no homogeneous mineral compositions). Consequently, we disagree with this earlier interpretation.

Stöffler et al. (1980) define an impact-melt breccia as "a rock containing lithic and mineral clasts embedded in an igneous-textured, crystalline matrix." We interpret SaU 300 as a clast-bearing, polymict impact-melt breccia with an olivine-rich anorthositic norite bulk composition. This interpretation is based on its subophitic matrix texture, its variable lithic clast population, its depletion in trapped solar wind components, and its lack of any visible regolithic components (e.g., agglutinates, glassy spherules). The low noble gas content is probably a result of the plutonic origin of lithic and mineral clasts (which would have a low solar wind component due to burial) and the melt origin of the matrix, where the heat of fusion would have driven off any solar wind component.

Shock History

SaU 300 is a polymict impact-melt breccia that records evidence of multiple impact events. We have distinguished at least three distinct shock-generated assemblages: 1) a prematrix assemblage comprising lithic and mineral clasts that have undergone different degrees of shock. The clasts retain evidence of having been shocked between 5–28 GPa (shock stages S1–S2), based on the summary of Hiesinger and Head (2006); 2) a shock melting event that produced the fine-grained igneous matrix of the meteorite. Formation of the matrix would have required relatively high shock pressures (>60 GPa). This event also entrained the lithic and mineral clasts that presumably formed part of the target terrain. It is conceivable that the clasts were generated by the same shock event that formed the melt, but this is considered unlikely, at least for all lithic and mineral clasts; and 3) a postmatrix assemblage comprising localized shock excursion effects including shock veins, melt pockets, and clast margin-matrix contacts, all of which exhibit melting and glass formation. The host rock margins of the veins and pockets show local shock-induced transformations (e.g., maskelynitization). The excursions attained 28–45 GPa (shock stage S2–S3).

The formation of SaU 300 can be summarized as follows:

1. An impact event brecciated an area of highland crust comprising various lithologies. The impact event excavated a basin and created impact melt, which entrained clasts of the various target lithologies. Mineral fragments and lithic clasts record varying degrees of shock metamorphism, ranging from strong mosaicism with multiple sets of planar fractures to undulose extinction and irregular fracturing. Retention of these shock features indicates that the thermal energy of the host melt was insufficient to erase them through annealing. The edges of mineral and lithic clasts range from sharp to embayed, revealing variations in the degree of interaction with the molten matrix.
2. Following shock melting and clast incorporation, the matrix crystallized and cooled slowly enough to form the subophitic texture observed. Deutsch and Stöffler (1987) estimate that in order to produce a subophitic-textured impact-melt rock, an impact crater must be larger than ~5 km in diameter. However, the matrix of SaU 300 has a microscopic igneous texture and includes pigeonite, indicating that it was formed in a small crater (5–10 km in diameter), at the margins of a larger impact-melt body, or cooled as part of a thinner ejecta blanket.
3. A later shock event generated the shock veins and melt pockets that pervade the rock, and that may have ejected the rock from the surface of the Moon. Maskelynite is restricted in occurrence to areas in direct contact with the melt pockets and shock veins (Figs. 6c and 6d). Patchy maskelynitization otherwise occurs in anorthositic clasts (Fig. 6b).

Shock Classification

Based on the shock classification summary of Hiesinger and Head (2006), formation of the melt that cooled to form the matrix would have required shock pressures >60 GPa (shock stage S4). The presence of melt pockets and veins indicates a later shock excursion event, which locally attained shock pressures of 28–45 GPa (shock stage S2–S3). Localized shock melting may have occurred during spallation and ejection from the lunar near-surface. This is the case for most of the Martian meteorites, where shock veins and melt pockets are restricted to the highly shocked (>20 GPa) shergottites (basalts, olivine-phyric basalts, and lherzolitic basalts) (Greshake et al. 2004; Mikouchi et al. 2004; Fritz et al. 2005). Lightly shocked nakhlites, although presumably ejected by the same spallation mechanism, do not contain localized shock melting features.

Although a quantitative measurement of the equilibration shock pressure and corresponding post-shock temperature is lacking for SaU 300, it can be estimated based on observed shock effects in plagioclase (partial isotropism, undulose extinction, planar fractures, maskelynitization) and clinopyroxene (mechanical twinning, moderate mosaicism). SaU 300 can be assigned to a shock stage that is not dependent on measurement of the absolute shock pressure, but relative to an existing shock recovery database (see Hiesinger and Head 2006 for compiled data). The bulk of the mineral and lithic clasts belong to shock stage 1b of Stöffler et al. (1980), which corresponds to an equilibration shock pressure of 20–22 GPa and a post-shock temperature of

200 °C. Later shock melts, which crosscut the host rock, indicate local shock excursions of 28–45 GPa and elevated temperatures (high enough to melt the rock). Similar to the Martian meteorites, localized shock melt products (veins and pockets) are generally attributed to heterogeneous shock excursions resulting from shock and frictional melting (veins). Possible scenarios for melt pocket formation, based on the presence of high-pressure mineral polymorphs (Beck et al. 2004) and trapped atmosphere (e.g., Bogard and Johnson 1983; Walton et al. 2007), involve injection of extraneous molten material into cracks and fractures in the host rock in the vicinity of the impact, and in situ localized melting by shock impedance contrasts as a result of the polycrystalline nature of the target material. For the latter mechanism, the most extreme case would represent collapse of pore space in the host rock. Evidence for local shock excursions includes maskelynite formation and the isolated nature of the melts. For the veins, shearing and displacement of neighboring host rock phases indicates a frictional component to their formation. The observation that SaU 300 was locally strongly shocked by the ejection event is consistent with the observation that SaU 300 was excavated from depth (i.e., not from the lunar regolith).

SaU 300 Source Location

The absence of any visible mare or clastic material rich in potassium, rare earth elements (REE), or phosphorus (i.e., KREEP), and the abundance of plagioclase-dominated lithic clasts, suggests a provenance far removed from the large mare basins and the Th-rich Procellarum KREEP Terrane (PKT). SaU 300 may have been derived from the far-side Feldspathic Highlands Terrane (FHT) and, if so, it provides information about a region remote from the Apollo and Luna sites.

Pairing

This investigation indicates that SaU 300 is compositionally unique and thus not paired with any lunar meteorite recovered to date. Other feldspathic impact-melt breccias include Dhofar (Dho) 026, Northwest Africa (NWA) 482, Dar al Gani (DaG) 400, NWA 2200, Dho 1428, and Dho 303. Compared to these samples, SaU 300 is rich in Fe and Mg and depleted in Ca and Al, indicating that it probably contains more mafic and fewer feldspathic phases. Dho 026 is clast-poor and contains basaltic melt spherules (Cohen et al. 2001). DaG 400 contains regolith components, such as agglutinates and glass spherules (Zipfel et al. 1998). NWA 482 is depleted in TiO_2 (<0.13 wt%) and FeO (<4 wt%) and rich in Al_2O_3 (29–31 wt%) (Dauber et al. 2002). Dho 303 contains very low-Ti (VLT) basalt clasts and KREEP-rich glass (Nazarov et al. 2002), making it an unlikely pair for SaU 300. The bulk rock composition of SaU 300 is unlike any previously described feldspathic lunar meteorite. It is mineralogically similar to most highlands meteorites in that it is dominated by anorthite, olivine, and pyroxenes, and contains no phosphorus or REE-enriched minerals. However, SaU 300 falls between the "mingled meteorite" and the "highland meteorite" fields on most major and minor element plots (Fig. 11).

CONCLUSIONS

SaU 300 was previously misclassified as an anorthositic regolith breccia possessing a granulitic texture (Bartoschewitz et al., unpublished data). Here we classify it as a polymict crystalline impact-melt breccia. Its bulk composition, as determined by the raster scanning of two thin sections, is olivine-rich anorthositic norite, with an igneous matrix composition of a troctolitic anorthosite. This polymict breccia is rich in meteoritic metal, indicating a history dominated by impact events. It lacks any mare or KREEP-rich lithologies, which favors a provenance far removed from the PKT, possibly in the farside FHT.

SaU 300 has undergone at least two episodes of shock One event was responsible for forming the impact-melt matrix and entraining the lithic and mineral clasts, which themselves exhibit variable shock histories. A second event resulted in the formation of shock melt veins and pockets, as well as local phase transformation of anorthite to maskelynite. The variety and variable shock states of the lithic and mineral fragments indicate that the target area experienced multiple impact events prior to formation of the enclosing igneous matrix.

The mineral and lithic clasts of SaU 300 exhibit shock stages S1–S2 (mainly S1b) effects (5–28 GPa). Impact melting (to generate the igneous matrix) required shock pressures of >60 GPa (shock stage >S4). Subsequent shock excursions, most likely associated with ejection of the meteorite from the lunar surface, reached shock pressures of 28–45 GPa (shock stages S2–S3).

On the basis of its compositional uniqueness, we propose that SaU 300 represents a new lunar meteorite that is unpaired with currently known samples.

Acknowledgments–This research has been supported by a Natural Sciences and Engineering Research Council of Canada (NSERC) CGS-M graduate award to JAH, an NSERC Post-Doctoral Fellowship award, Alberta Ingenuity Fund award, and Canadian Space Agency Supplement to ELW, and NSERC Discovery and Canada Research Chair grants to JGS. Rainer Bartoschewitz kindly loaned the two thin sections used for this study. Thanks to Douglas Hall (UNB) for ASEM assistance and George Braybrook and Sergei Matveev (UA) for FE-SEM and EMP support. B. Jolliff, T. Mikouchi, and R. Korotev are thanked for reviewing an earlier version of this paper. Planetary and Space Science Centre publication 55.

Editorial Handling—Dr. Randy Korotev

REFERENCES

Ashwal L. 1998. Anorthosites: Classification, mythology, trivia, and a simple unified theory. LPI Technical Report #88-06. Houston, Texas: Lunar and Planetary Institute. pp. 30–32.

Beck P., Gillet P., Gautron L., Daniel I., and El Goresy A. 2004. A new natural high-pressure (Na,Ca)-hexaluminosilicate ($[Ca_xNa_{1-x}]Al_{3+x}Si_{3-x}O_{11}$) in shocked Martian meteorites. *Earth and Planetary Science Letters* 219:1–12.

Bogard D. D. and Johnson P. 1983. Martian gases in an Antarctic meteorite? *Science* 221:651–654.

Cohen B. A., Taylor L. A., and Nazarov M. A. 2001. Lunar meteorite Dhofar 026: A second generation impact melt (abstract #1404). 32nd Lunar and Planetary Science Conference. CD-ROM.

Cohen B. A., James O. B., Taylor L. A., Nazarov M. A., and Barsukova L. D. 2004. Lunar highland meteorite Dhofar 026 and Apollo sample 15418: Two strongly shocked, partially melted, granulitic breccias. *Meteoritics & Planetary Science* 39:1419–1447.

Dauber I. J., Kring D. A., Swindle T. D., and Jull A. J. T. 2002. Northwest Africa 482: A crystalline impact-melt breccia from the lunar highlands. *Meteoritics & Planetary Science* 37:1797–1813.

Day M. D. J, Taylor L. A., Floss C., Patchen A. D., Schnare D. W., and Pearson D. G. 2006. Comparative petrology, geochemistry, and petrogenesis of evolved low-Ti lunar mare basalt meteorites from the LaPaz Icefield, Antarctica. *Geochimica et Cosmochimica Acta* 70:1581–1600.

Deutsch A. and Stöffler D. 1987. Rb-Sr analyses of Apollo 16 melt rocks and a new age estimate for the Imbrium basin: Lunar basin chronology and the early heavy bombardment of the Moon. *Geochimica et Cosmochimica Acta* 51:1951–1964.

Fritz J., Artemieva N., and Greshake A. 2005. Ejection of Martian meteorites. *Meteoritics & Planetary Science* 40:1393–1411.

Gnos E., Hofmann B. A., Al-Kathiri A., Lorenzetti S., Eugster O., Whitehouse M. J., Villa I. M., Jully A. J., Eikenberg J., Spettel B., Krähenbühl U., Franchi I. A., and Greenwood R. C. 2004. Pinpointing the source of a lunar meteorite: Implications for the evolution of the Moon. *Science* 305:657–659.

Greshake A., Fritz J., and Stöffler D. 2004. Petrology and shock metamorphism of the olivine-phyric shergottite Yamato-980459: Evidence for a two-stage cooling and a single-stage ejection history. *Geochimica et Cosmochimica Acta* 68:2359–2377.

Hewins R. H. and Goldstein J. I. 1975. The provenance of metal in anorthositic rocks. Proceedings, 6th Lunar Science Conference. pp. 343–362.

Hiesinger H. and Head J. W. Jr. 2006. New views of lunar geoscience: An introduction and overview. In *New views of the Moon*, edited by Jolliff B. L., Wieczorek M. A., Shearer C. K., and Neal C. R. Reviews in Mineralogy and Geochemistry, vol. 60. Chantilly, Virginia: Mineralogical Society of America. pp. 1–67.

Hsu W., Guan Y., Ushikubo T., Bartoschewitz R., Zhang A., Kurtz Th., and Kurtz P. 2006. Petrology and REE geochemistry of the lunar meteorite Sayh al Uhaymir 300 (abstract #5200). *Meteoritics & Planetary Science* 41:A79.

Jolliff B. L., Gillis J. J., Haskin L. A., Korotev R. L., and Wieczorek M. A. 2000. Major lunar crustal terranes: Surface expressions and crust-mantle origins. *Journal of Geophysical Research* 105: 4197–4216.

Korotev R. L. 2005. Lunar geochemistry as told by lunar meteorites. *Chemie der Erde* 65:297–346.

Lindsley D. H. and Anderson D. J. 1983. A two-pyroxene thermometer. *Journal of Geophysical Research* 88:A887–A906.

Lofgren G. 1980. Experimental studies on the dynamic crystallization of silicate melts. In *Physics of magmatic processes.* Princeton, New Jersey: Princeton University Press. pp. 487–551.

Mikouchi T., Koizumi E., McKay G., Monkawa A., Ueda Y., Chokai J., and Miyamoto M. 2004. Yamato-980459: Mineralogy and petrology of a new shergottite-related rock from Antarctica. *Antarctic Meteorite Research* 17:13–34.

Nazarov M. A., Demidova S. I., Patchen A., and Taylor L. 2002. Dhofar 301, 302, and 303: Three new lunar highland meteorites from Oman (abstract #1293). 33rd Lunar and Planetary Science Conference. CD-ROM.

Papike J., Taylor L., and Simon S. 1991. Lunar minerals. In *Lunar sourcebook: A user's guide to the Moon,* edited by Heiken G., Vaniman D., and French B. M. New York: Cambridge University Press. pp. 183–284.

Spray J. G. and Rae D. A. 1995. Quantitative electron-microprobe analysis of alkali silicate glasses: A review and user guide. *Canadian Mineralogist* 33:323–332.

Stöffler D., Knöll H-D., Marvin U. B., Simonds C. H., and Warren P. H. 1980. Recommended classification and nomenclature of lunar highland rocks—A committee report. Proceedings, Conference on the Lunar Highlands Crust. New York: Pergamon Press. pp. 51–70.

Walton E. L., Kelley S. P., and Spray J. G. 2007. Shock implantation of Martian atmospheric argon in four basaltic shergottites: A laser probe $^{40}Ar/^{39}Ar$ investigation. *Geochimica et Cosmochimica Acta* 71:497–520.

Walton E. L., Shaw C., Cogswell S., and Spray J. G. 2006. Crystallization rates of shock melts in three Martian basalts: Experimental simulation with implications for meteoroid dimensions. *Geochimica et Cosmochimica Acta* 70:1059–1075.

Warren P. H., Taylor G. J., Keil K., Kallemeyn G. W., Rosener P. S., and Wasson J. T. 1983. Sixth foray for pristine non-mare rocks and an assessment of the diversity of lunar anorthosites. Proceedings, 13th Lunar and Planetary Science Conference. pp. A615–A630.

Warren P. H. and Kallemeyn G. W. 1991. The MacAlpine Hills lunar meteorite and implications of the lunar meteorites collectively for the composition and origin of the Moon. *Geochimica et Cosmochimica Acta* 55:3123–3138.

Wlotzka F. 1993. A weathering scale for ordinary chondrites (abstract). *Meteoritics* 28:460.

Zipfel J., Spettel B., Palme H., Wolf D., Franchi I., Sexton A. S., Pillinger C. T., and Bischoff A. 1998. Dar al Gani 400: Chemistry and petrology of the largest lunar meteorite (abstract). *Meteoritics & Planetary Science* 33:A171.